3D Particle Tracking Velocimetry applied to platelet-size particles in red blood cells suspensions flows through square microchannels

Coutinho, Gonçalo; Rossi, Massimiliano; Moita, Ana ; L. N. Moreira, António

Published in:
Proceedings of the 20th International Symposium on Application of Laser and Imaging Techniques to Fluid Mechanics

Publication date:
2022

Document Version
Publisher's PDF, also known as Version of record

3D Particle Tracking Velocimetry applied to platelet-size particles in red blood cells suspensions flows through square microchannels

Gonçalo Coutinho[1,*], Massimiliano Rossi[2], Ana Moita[1,3], António L. N. Moreira[1]

1: IN+ Center for Innovation, Technology and Policy Research, Instituto Superior Técnico, Portugal
2: Department of Physics, Technical University of Denmark, Denmark
3: CINAMIL - Centro de Investigação Desenvolvimento e Inovação da Academia Militar, Academia, Portugal
*Corresponding author: goncalo.coutinho@tecnico.ulisboa.pt

Keywords: 3D Particle tracking velocimetry, General defocusing particle tracking, Red blood cells, Platelet-size particles, 3D Flow characterization

ABSTRACT

General defocusing particle tracking (GDPT) method is used to characterize the motion of platelet-size particles within red blood cell (RBC) suspension flows through straight-square microchannels. The method is able to characterize the three-dimensional (3D) nature of particle-RBC interactions, however the measurement depth is limited by the height of the microchannel and hematocrit level (Hct). The RBC mask the particle images and detection becomes impossible above a limit depth. The pressure-driven flow is characterized by velocity distributions and 3D trajectories of platelet-size particles within the RBC suspensions. At large hematocrit levels (Hct=30 %), the velocity distribution exhibits a blunter profile typical of blood flow in capillary-size microchannels. In addition, the interplay between blood viscosity and pressure-driven flow causes the velocity magnitude to decrease, in the center region, with increasing hematocrit. The platelet-size particles exhibit larger velocity fluctuations along the spanwise and vertical directions as Hct is increased, both inside the RBC-rich region and cell-free layer (CFL). On one hand, inside the RBC-rich zone the increasing number of flowing RBC leads to more frequent particle-RBC collisions. On the other hand, even though the particle movement inside the CFL is confined between the boundary of the RBC and the wall of the microchannel, as the thickness of the CFL decreases (i.e. increasing Hct) the collisions with RBC become more frequent. To the authors knowledge, these results represent the first experimental characterization of 3D platelet-size particle behaviour and near-wall dynamics within RBC-suspensions, and it paves the way for more detailed particle-cell flows characterization.

1. Introduction

Red blood cells (RBC) in blood vessels flow mainly around the center-line, thereby creating a RBC-depleted zone in the near-wall region known as cell-free layer (CFL), where rigid particles such as white blood cells, platelets or synthetic particles are forced to travel (Carboni et al., 2016; Vahidkhah et al., 2014). This near-wall circulation of platelets is essential to survey the condition of the

vessel wall and to respond to injuries. Therefore, the characterization of the transport and near-wall dynamics of rigid particles within the blood flow is fundamental to comprehend platelets motion and design new drug-carrying particles. Despite existent three-dimensional (3D) numerical simulations (Vahidkhah et al., 2014), so far no experimental study has characterized the 3D nature of particle-RBC dynamics.

In the present work, the general defocusing particle tracking (GDPT) method (Barnkob & Rossi, 2020; Rossi & Barnkob, 2020) is used to uncover the 3D nature of the particle-RBC flows in capillary-size microchannels. To mimic platelets, rigid-fluorescent polystyrene (PS) microspheres ($d_p = 2.5\,\mu$m) are added to RBC suspensions. First, the bias error in GDPT measurements due to the field curvature is corrected using the particle trajectories. The impact of the curvature of the focal plane is significant and can lead to erroneous interpretation of particle trajectories (Cierpka et al., 2010; Rossi & Barnkob, 2020). Then, the velocity distributions from the corrected particle coordinates are analysed for different hematocrit levels (Hct), and ultimately, preliminary results on the particle behaviour within RBC-suspensions are provided.

2. Materials and methods

2.1. Experimental setup

The general schematic of the experimental setup is provided in Fig. 1(a). The microchannel was placed on the working stage of an epi-fluorescent inverted microscope (DM IL LED, Leica Microsystems GmbH) equipped with a high-speed camera (HighSpeedStar 4G, LaVision GmbH). The system was operated with a $\times 20/0.4$ objective lens (NPlan Epi, Leica Microsystems GmbH) which yielded a spatial resolution of 0.85 µm/pixel. The present configuration used a backlight illumation provided by a high-power green LED (Solis-525C, Thorlabs Inc.) and a filter cube for fluorescence imaging (Excitation:BP 525/50 nm; Dichroic: 570nm and Emission: 620/60 nm).

The RBC suspensions were prepared from bovine washed RBC (IBORBC100P, Innovative Research Co.). The selected hematocrit levels Hct=$10,\ 20,\ 30\,\%$ were adjusted by diluting the RBC in phosphate-buffered saline (PBS) ($\times 1.0$, ph=7.4, FisherScientific Co.) (Carboni et al., 2016). Then, platelet-size fluorescent microspheres (530/607 nm, PS-FluoRed, MicroParticles GmbH) with nominal diameter of $2.47\,\mu$m were added to each solution. To avoid misleading analysis of the data, a single solution was prepared for each Hct. All measurements were performed in a single microchannel with square cross-sectional area of $w_{\text{ch}} \times h_{\text{ch}} = 50 \times 50\,\mu\text{m}^2$ and length of $l_{\text{ch}} = 58.5\,$mm (CS-10000087, Darwin Microfluidics). The microchannel is made of a rigid polymer (Topas COC) with bottom wall thickness of 140 µm which was enhanced by placing a 1-mm-thick glass microscope slide underneath (D100001, Deltalab), see Fig. 1(a).

In all measurements the pressure-driven flow was imposed by hydrostatic pressure. To obtain the desired flow rate, an offset (h_{p}) between the inlet and collection reservoir was set by a millimeter stage (Edmund Optics Co.). The reference flow rate was determined by measuring the Poiseuille

flow of a PBS solution in the absence of cells (no-RBC): $\bar{v_x} = 1.4\,\mathrm{mm/s}$, $Q_\mathrm{p} = 0.22\,\mu\mathrm{L/min}$. To ensure the reproducibility of the results, the data were acquired twice per hematocrit level. Between measurements, the whole system was flushed and the microchannel rinsed with distilled water for 10 minutes. Additionally, the RBC suspensions were gently agitated before each measurement to avoid sedimentation.

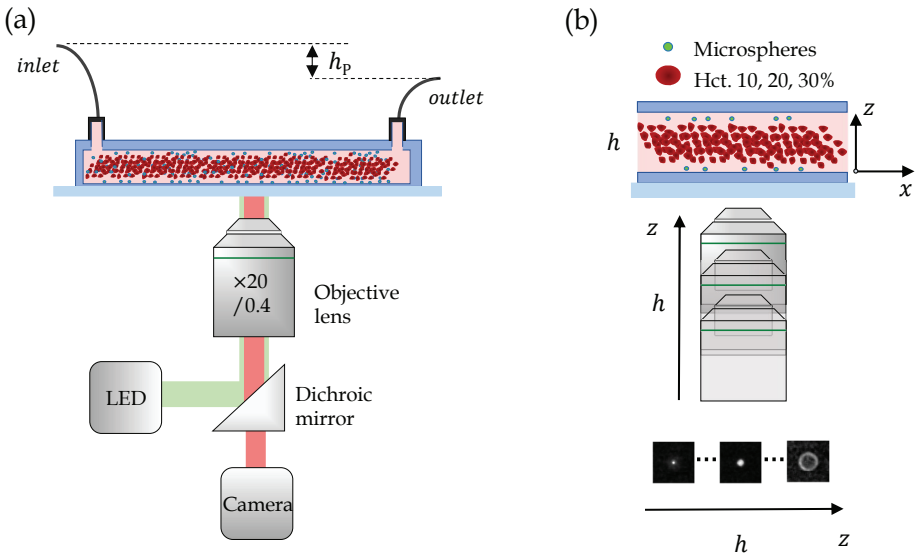

Figure 1. (a) Schematic of the experimental setup used to perform the GDPT measurements. (b) Schematic of the acquisition of the calibration image stack.

2.2. General defocusing particle tracking

The flow fields were characterized with a single-camera 3D particle velocimetry method, referred to as general defocusing particle tracking (GDPT) (Barnkob & Rossi, 2020; Rossi & Barnkob, 2020). For optical setups providing particle images that vary solely with depth coordinate, the method takes advantage from the depth-dependent shape of particle images to determine the depth position. To this aim, prior to experiments, the measurement volume is mapped with a calibration image stack. Typically, a tracer particle sedimented at the bottom of the microchannel is recorded at different depth positions by moving the objective lens at different focus positions, see Fig. 1(b). Briefly, the particle detection and coordinates estimation was performed by comparing experimental and calibration images with normalized cross-correlation (Lewis, 1994). The particle tracking was performed with the nearest-neighbour algorithm, since the particle density was low (Malik et al., 1993). This was performed using DefocusTracker (Barnkob & Rossi, 2021), an open-source GDPT software, available at following link: `https://gitlab.com/defocustracking`.

For the measurements reported here, the optical setup provided a measurement depth $h = 100\,\mu m$, hence the flow inside the microchannel could be characterized in a single measurement and no scanning procedures were needed. In each measurement, the flow was recorded using dark-field images of the platelet-size particles (2500 Frames @ f_{cam}= 50 Hz). Additionally, bright-field images of the RBC were obtained to characterize the thickness of the CFL (δ_{CFL}). For each solution (i.e. Hct), the calibration image stack was obtained by taking images of a particle resting at the bottom of the microchannel, and adjusting the depth position by moving the objective lens with an in-house motorized focus controller at a constant step size of $1\,\mu m$ (see Fig. 1(b)). To provide a general idea of the 3D extent of the present measurements, Fig. 2(a) depicts 3D trajectories of platelet-size particles within a RBC suspension at Hct=10 %. The high concentration of RBC in all RBC-suspension flows masks the images of the tracer particles, hence only half the height of the microchannel was considered ($h_{ch}/2$). Figure 2(b) shows the maximum detected height for different cases.

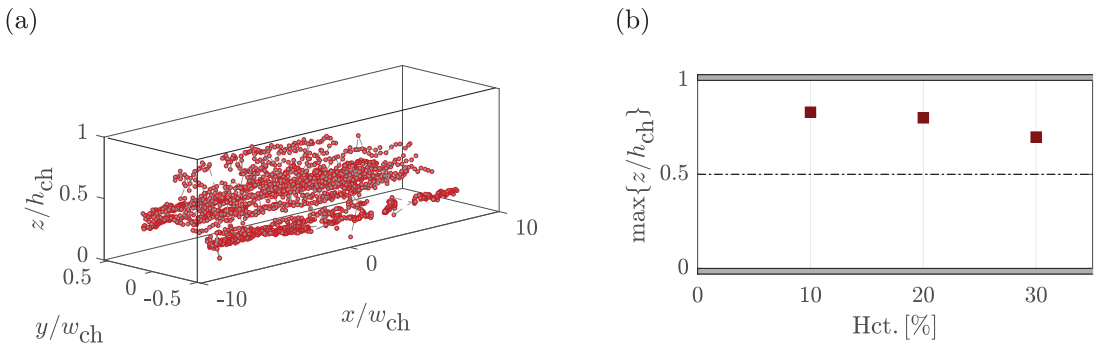

Figure 2. (a) Sample particle trajectories from platelet-size particle flowing within RBC suspensions (Hct=10 %). (b) Maximum detected depth-coordinate max$\{z/h_{ch}\}$ as function of hematocrit level Hct. The gray blocks represent the walls of the microchannel.

2.3. Correction of bias error in the GDPT measurements

In general, the estimated depth coordinate z/h from a GDPT evaluation can be biased by the field curvature aberration (Rossi & Barnkob, 2020). This optical aberration is a result of the surface curvature and refractive index of the objective lens, and causes a geometrical distortion that transforms a planar into a curved focal plane (Born & Wolf, 1975). As a consequence, the depth z/h at which the object is in-focus will depend on the lateral distance to the optical axis. In practice, this means that, for instance, all tracer particles located on a horizontal plane at a given depth z/h, will appear as sited on a curved surface instead on an ideal horizontal plane (Cierpka et al., 2010).

To account for this bias, Rossi & Barnkob (2020) used a calibration image stack including multiple sedimented particles spread across the bottom of the microchannel to obtain the curved surface

that resembled the field curvature. In the present work, a new method based on the estimated particle trajectories is applied to derive the curved surface. Since the measurements were performed in straight microchannels, the particle trajectories for a pressure-driven flow must be straight (Bruus, 2008). However, with the influence of the field curvature, the measured particle trajectories exhibit a non-physical curved profile. Under this condition, the particle trajectories are used to determine a parabolic surface that fits the curvature of the focal plane

$$f_z(x, y) = p_{00} + p_{10}x + p_{01}y + p_{11}xy + p_{20}x^2 + p_{02}y^2. \tag{1}$$

Based on the fitted curved surface $f_z(x, y)$, the field curvature correction factor is obtained by finding the difference between $f_z(x, y)$ and the horizontal plane tangent to $f_z(x, y)$ at the center of the field-of-view (FOV) ($x = y = 0$).

For the present measurements, since the width of the microchannel w_{ch} was significantly smaller than the size of the FOV, the field curvature was only detected in the flow direction x. The contribution was found to be non-negligible and up to $3.4\,\%$ of the measurement depth z/h. To illustrate it, Figures 3(a) and 3(b) depict the pre- and post-corrected particle coordinates, respectively.

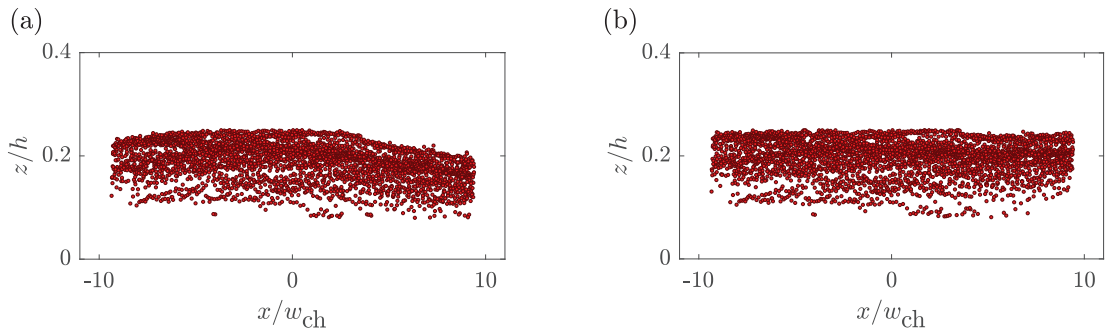

Figure 3. Example of the impact of field curvature on the estimated particle coordinates from a GDPT evaluation (Hct=20 %). (a)-(b) Pre- and post-corrected particle coordinates with the estimated curved map, respectively. Notice here, the depth coordinate is shown as a function of the measurement depth h.

Figures 3(b) and 3(b) show that the bias due to the field curvature can mask or alter the biophysical interpretation of particle-cell interactions, therefore, this optical aberration must be accounted for when performing GDPT measurements on this type of flows.

Furthermore, the horizontal plane was used to find the three orthogonal vectors that define the orientation of the measurement volume, and subsequently rotate the particle coordinates so that the measurement volume is aligned with the coordinate axis (x, y, z). Solely, the orientation of the measurement volume does not represent a contribution to the bias error, however when neglected it may represent an error of a few microns in the 3D particle position.

3. Results

3.1. Flow characterization

The streamwise velocity distribution v_x of the platelet-size particles is measured for three RBC suspensions (Hct = 10, 20, 30 %) in similar flow conditions imposed by a constant pressure drop ΔP. The flow is analysed along the spanwise y and vertical z directions, the latter being restricted to half the height of the microchannel $z/h_{\mathrm{ch}} = 0.5$, see Fig. 4(a)-(b). For comparison, the velocity profiles were fitted to an empirical equation derived from the solution for Poiseuille flow in straight-squared microchannels

$$v_x = v \cdot \left(\frac{\cosh(0.5^m) - \cosh(|y_{\mathrm{i}}^*|^m)}{\cosh(0.5^m) - 1} \right) + v_0, \tag{2}$$

where v and v_0 are the fitting parameters based on the velocity distributions, and m is a fitting parameter based on the velocity profile bluntness. Here, the coordinates y_{i}^* are normalized with the width w_{ch} and height h_{ch} of the microchannel, for the y- and z directions, respectively. Details on the mathematical derivation are provided in Sherwood et al. (2014).

With increasing hematocrit, the velocity distributions show a deviation from the classical Poiseuille flow of a Newtonian fluid (Bruus, 2008), see Fig. 4(a)-(b): whereas, at low hematocrit (Hct=10 %), the distribution resembles a parabolic profile, for higher concentrations of RBC the velocity distribution starts to exhibit a plateau in the center region. This blunter profile is characteristic of blood-flow suspensions in capillary-size microchannels and has been reported in previous numerical (Bagchi, 2007) and experimental studies (Tatsumi et al., 2019).

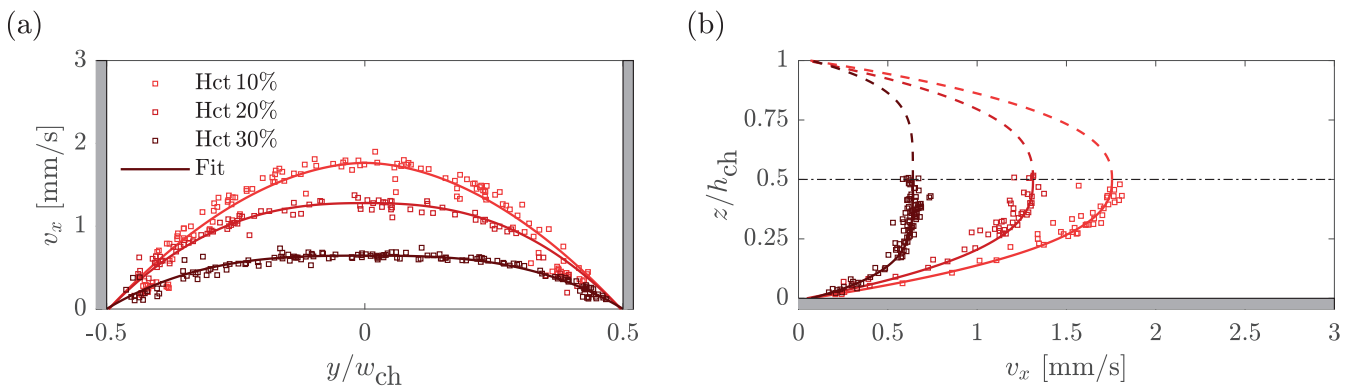

Figure 4. (a)-(b) Distribution of the streamwise velocity component v_x of platelet-size particles in RBC-suspension flow at varying hematocrit (Hct = 10, 20, 30 %) along the spanwise y and vertical z directions, respectively. The gray blocks represent the walls of the microchannel.

A decrease in the maximum velocity max$\{v_x\}$ is also detected with increasing Hct, which may be related to the increasing blood viscosity with larger RBC concentration (Fitzgibbon et al., 2015), see Fig. 5(a). As the fluid becomes more viscous, larger pressure drops are required to drive the flow at the same velocity. To shed light into the interplay between the viscosity of RBC suspensions and estimated velocity, the relative viscosity μ_{rel} is estimated for the different cases. Following the work of Bagchi (2007), the viscosity of the RBC-suspensions is expressed as an apparent viscosity μ_{app} using the analytical solution of a Poiseuille flow in a microchannel with squared cross-section (Bruus, 2008) and it is given by

$$\mu_{\text{app}} = \frac{h_{\text{ch}}^3 w_{\text{ch}} \Delta P}{12QL}\left[1 - \sum_{n,odd}^{\infty} \frac{1}{n^5}\frac{192}{\pi^5}\frac{h}{w}\tanh\left(n\pi\frac{w}{2h}\right)\right] \tag{3}$$

where h_{ch} and w_{ch} are the height and width of the microchannel, respectively, $\Delta P/L$ the imposed pressure gradient and Q the volumetric flow rate. To obtain the relative viscosity μ_{rel}, the apparent viscosity of RBC-suspensions is compared to the viscosity of a Poiseuille flow without flowing RBC, see Eq. (4). For the present study, a solution of PBS was used. The mathematical expression is as follows:

$$\mu_{\text{rel}} = \frac{\mu_{\text{app}}}{\mu_{\text{PBS}}} = \frac{Q_{\text{PBS}}}{Q_{\text{RBC}}}, \tag{4}$$

where Q_{RBC} and Q_{PBS} represent the flow rate with and without flowing RBC, respectively.

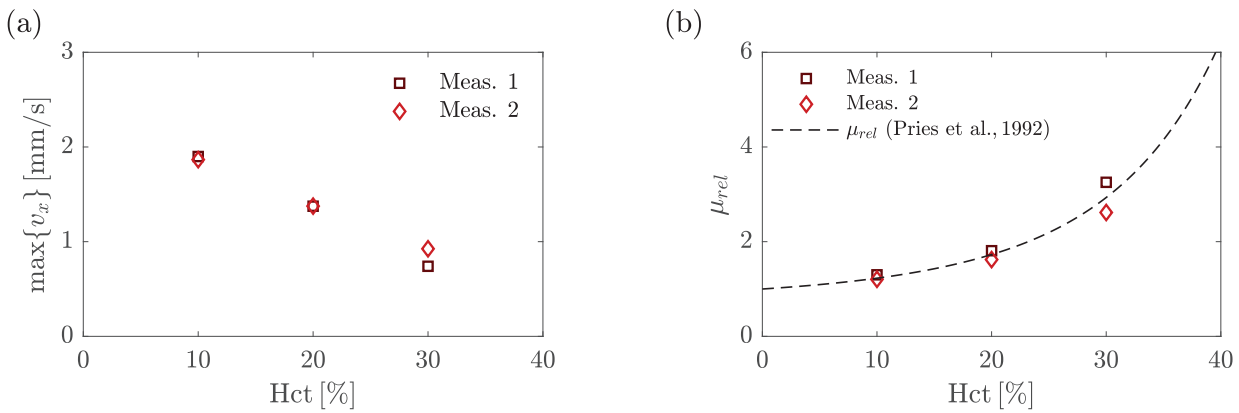

Figure 5. (a) Estimated maximum velocity max$\{v_x\}$ of the platelet-size particles in RBC-suspension flows with increasing Hct. (b) Relative viscosity μ_{rel} with varying Hct. The different markers refer to results from two different measurements (Meas. 1, Meas. 2) for the same flow conditions.

Figure 5(b) depicts the evolution of the relative viscosity as a function of the hematocrit level (Hct). The viscosity of the RBC suspensions increases considerably with Hct which is in agreement with

the measured velocity from Fig. 4(a)-(b). To compare the present measurements with those reported in previous studies, the relative viscosity was fitted to the empirical model given by Pries et al. (1992):

$$\mu_{\text{rel}} = 1 + B \cdot [(1 - \text{Hct})^C - 1], \tag{5}$$

where B and C are fitting parameters and Hct is the hematocrit level. The fitted curve shown in Fig. 5(b) demonstrates the good agreement between the present experimental data and expected hematocrit-relative viscosity relation (r^2=0.930). Furthermore, the reproducibility of the present results can be evaluated from the maximum velocity and relative viscosity obtained from two measurements (Meas. 1, Meas. 2) for the same flow conditions, see Fig. 5(a)-(b).

In general, the concept of relative viscosity provides a measure of the fluid viscosity as function of the hematocrit level (Pries et al., 1992; Bagchi, 2007), and hence it can be used as a first approximation to evaluate the overall decrease in the maximum velocity. However, this empiric model fails when studying the local viscosity in RBC-suspension flows due to its heterogeneous distribution (Sherwood et al., 2014). Since the viscosity directly relates to the aggregation of RBC, it is expected to take larger values within the RBC-rich region, whilst taking lower values within the RBC-depleted region (Yeom et al., 2014). This feature can be correlated with the velocity distributions from Fig. 4(a)-(b). Within the RBC-depleted region i.e., within the CFL, the results show a relatively high and comparable velocity magnitude for the considered Hct. On the other hand, as previously discussed, within the middlemost region the velocity magnitude decreases with increasing hematocrit level, thus with increasing viscosity.

4. Characterization of the platelet-size particles motion within RBC-suspension flows

To quantify the lateral v_y and vertical v_z motion of the platelet-size particles, the flow was divided in two regions of interest: RBC-rich zone and CFL. The particle behaviour was determined by the normalized root-mean square (RMS) of the lateral v_y and vertical v_z velocities. The results are shown in Fig. 6(a)-(b) for the RBC-rich zone and CFL, respectively.

Inside the RBC-rich region, the lateral and vertical velocity fluctuations is enhanced with increasing hematocrit, see Fig. 6(a). As the flow becomes more populated with RBC, the particle-RBC collision rate increases and accordingly, the platelet-size particles exhibit a larger motion in the cross-flow directions. Similar results are found for particles flowing inside the CFL, despite the decreasing CFL thickness δ_{CFL} with increasing Hct, see Fig. 6(b). Whereas inside the CFL the particle movement is limited by the RBC-boundary and wall of the microchannel, as the CFL thins the particle-RBC collisions become more frequent. This is supported on one hand by the slightly lower RMS velocity inside the CFL when compared to the RBC-rich region, see Fig. 6(a)-(b). On the other hand, the RMS velocity increases with Hct, and thus with decreasing CFL thickness. Similar results were found in the 3D computational simulation from Vahidkhah et al. (2014).

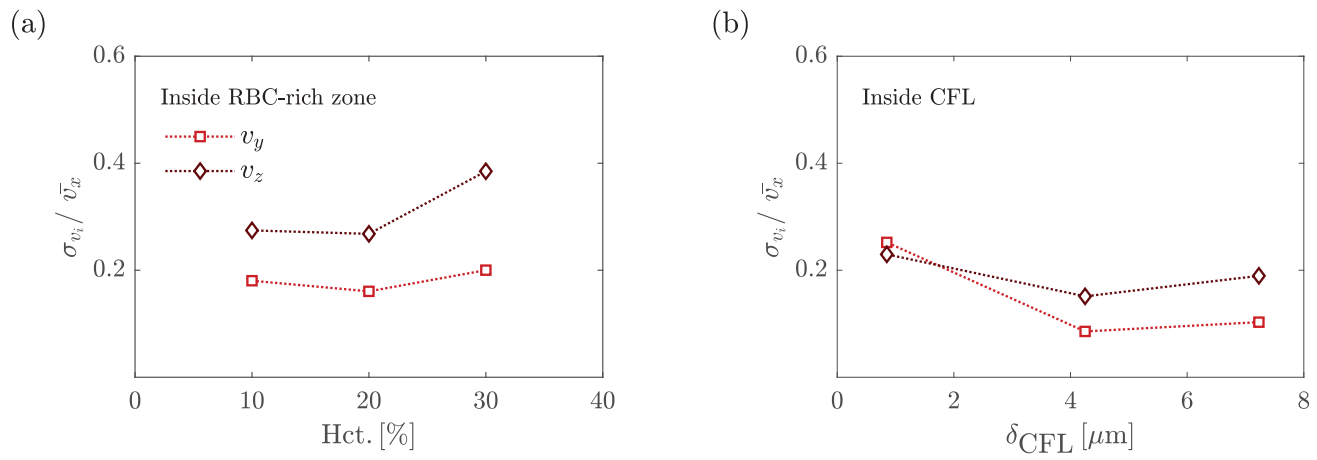

Figure 6. RMS velocity fluctuation of platelet-size particles movement inside the RBC-rich region and CFL for various RBCs suspensions (Hct = 10, 20, 30 %). The estimated CFL thickness (δ_{CFL}) from bright-field images of the RBCs flow is within the range 0.85 to 7.23 μm for Hct=30 − 10 %.

To further characterize the behaviour of the particles motion within the RBC-rich region and CFL, Fig. 7(a)-(d) show sample particle trajectories for both spanwise y and vertical z directions obtained at Hct=10, 30 %. The thickness of the CFL δ_{CFL} is represented by the dashed-black line. Here, three different types of trajectories are identified: Type A, B and C. Type A and type C denote trajectories of particles flowing within the RBC-rich and within the CFL, respectively. Type C represents the trajectory of marginating particles i.e., particles that are migrating from the RBC-rich region towards the near or inside the CFL due to the RBC-particle interaction (Vahidkhah et al., 2014).

For particles flowing inside the RBC-rich region (Type A), at Hct=30 % the particles undergo severe trajectory changes when compared to Hct=10 %, see Fig. 7(a)-(c). This particular behaviour is attributed to more frequent particle-RBC collisions for higher hematocrit as determined by the RMS velocity, see Fig. 6(a).

When travelling inside the CFL, the particles are confined between the boundary of the RBC and wall of the microchannel (Type B) (see Fig. 7(a)-(c)). These trajectories show more linear paths compared to those found inside the RBC-rich region. Such result evidences that generally once inside the CFL the particles are not allowed to re-enter the RBC region. Accordingly, for decreasing CFL thickness, the particles will be subjected to more collisions with the RBC boundary, and hence the larger RMS velocity shown in Fig. 6(b).

Ultimately, some particles travelling within the RBC-rich eventually are forced to migrate to near or inside the CFL (Type-C). As a consequence of the hemodynamics of RBC, rigid particles are expelled from RBC-rich region and forced to travel in the near-wall region. These trajectories are a clear evidence of the migration phenomenon of rigid particles within RBC-suspension flows known as margination (Carboni et al., 2016).

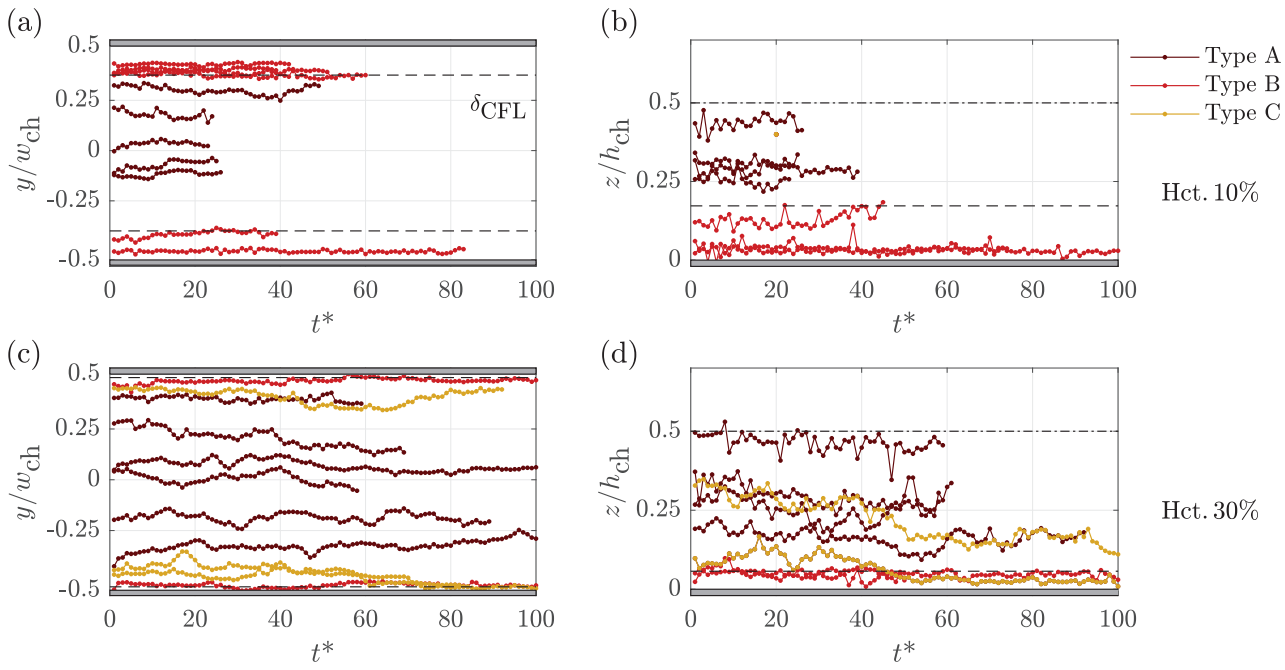

Figure 7. Sample trajectories of platelet-size particleswithin RBCs suspension flows at Hct. 10 % and Hct. 30 %. Type A - RBC-rich region; Type B - CFL; Type C - Marginating trajectories. (a) ,(b) Spanwise direction y **c** ,**d** Vertical direction z, respectively. The dashed-black line presents the thickness of the CFL δ_{CFL}.

5. Conclusions

The present work demonstrates that particle-RBC suspension flows can be characterized with GDPT measurements. First, it is shown that the field curvature aberration has a non-negligible contribution to the bias error and that for particle-cell experiments inside straight-square microchannels this bias can be corrected using the measured 3D particle trajectories. For the RBC-suspension flows, the measurement depth is limited by the depth of the microchannel and more importantly by the hematocrit levels. With increasing Hct, the number of flowing RBC start to mask the particle images and particle identification becomes impossible above a limit depth.

The estimated velocity distributions for the different Hct resemble the typical behaviour of blood flows in capillary-size microchannels. With increasing number of flowing RBCs, the velocity distributions deviate from a parabolic profile and start to exhibit a plateau in the center region. Moreover, a decrease in the maximum velocity is detected for increasing hematocrit. Since the flow was imposed with a constant pressure drop, the significantly larger viscosity at higher hematocrit levels leads to smaller velocity magnitude. Nonetheless, in future works, the difference between relative and local viscosity in RBC-suspension flows needs to be further discussed. The platelet-size particles behaviour within RBC-suspension flows is characterized by an increasing lateral and vertical movement as the hematocrit level is increased. This behaviour is observed for both RBC-

rich region and CFL, and it is promoted by the increasing number of flowing RBC. To the authors knowledge, this experimental study represents the first in-vitro 3D characterization of particle dynamics in RBC-suspension flows.

Acknowledgements

Gonçalo Coutinho (GC) acknowledges the PhD scholarship 2021.04780.BD attributed by Fundação para a Ciência e Tecnologia (FCT). Massimiliano Rossi acknowledges the financial support by the VILLUM foundation under the Grant No. 00036098. Gonçalo Coutinho, Ana Moita a António Moreira acknowledge Fundação para a Ciência e a Tecnologia (FCT) for partially financing the research trough Project Ref. PTDC/EME-TED/7801/2020.

References

Bagchi, P. (2007). Mesoscale simulation of blood flow in small vessels. *Biophysical Journal*, *92*(6), 1858–1877.

Barnkob, R., & Rossi, M. (2020). General defocusing particle tracking: fundamentals and uncertainty assessment. *Experiments in Fluids*, *61*(4), 110.

Barnkob, R., & Rossi, M. (2021). Defocustracker: A modular toolbox for defocusing-based, single-camera, 3d particle tracking. *Journal of Open Research Software*, *9*(1), 22.

Born, M., & Wolf, E. (1975). *Principles of optics*. Cambridge University Press.

Bruus, H. (2008). *Theoretical microfluidics*. Oxford University Press.

Carboni, E., Bognet, B., Bouchillon, G. M., Kadilak, A., Shor, L., Ward, M. D., & Ma, A. (2016). Direct tracking of particles and quantification of margination in blood flow. *Biophysical Journal*, *111*, 1487–1495.

Cierpka, C., Rossi, M., Segura, R., & Kähler, C. J. (2010). On the calibration of astigmatism particle tracking velocimetry for microflows. *Measurement Science and Technology*, *22*(1), 015401.

Fitzgibbon, S., Spann, A., Qi, Q., & Shaqfeh, E. G. (2015). In vitro measurement of particle margination in the microchannel flow: Effect of varying hematocrit. *Biophysical Journal*, *108*(10), 2601–2608. doi:

Lewis, J. (1994). Fast template matching. *Vision Interface*, *95*.

Malik, N., Dracos, T., & Papantoniou, D. (1993). Particle tracking velocimetry in three-dimensional flows - part ii: Particle tracking. *Experiments in Fluids*, *15*, 279-294.

Pries, A. R., Neuhaus, D., & Gaehtgens, P. (1992). Blood viscosity in tube flow: dependence on diameter and hematocrit. *American Journal of Physiology-Heart and Circulatory Physiology*, *263*(6), H1770–H1778. doi:

Rossi, M., & Barnkob, R. (2020). A fast and robust algorithm for general defocusing particle tracking. *Measurement Science and Technology*, *32*(1), 014001.

Sherwood, J. M., Holmes, D., Kaliviotis, E., & Balabani, S. (2014). Spatial distributions of red blood cells significantly alter local haemodynamics. *PLOS ONE*, *9*(6), e100473.

Tatsumi, K., Noguchi, S., Tatsumi, A., Kuriyama, R., & Nakabe, K. (2019). Particle and rigidized red blood cell concentration distributions in microchannel flows. *Physics of Fluids*, *31*(8), 082006.

Vahidkhah, K., Diamond, S. L., & Bagchi, P. (2014). Platelet dynamics in three-dimensional simulation of whole blood. *Biophysical Journal*, *106*(11), 2529–2540.

Yeom, E., Kang, Y., & Lee, S.-J. (2014). Changes in velocity profile according to blood viscosity in a microchannel. *Biomicrofluidics*, *8*, 034110.